

Understanding Collective Motion: Jamming and Crowd Dynamics

Dominic Bosco*: Oberlin College

Ethan Hobbs*: Carthage College

Rebecca Wayne*: University of Massachusetts-Lowell

James Worsham*: Baylor University

September 14, 2017

Abstract

Collective motion is key to understanding the behavior of different organisms and how they interact with each other as well as their surroundings. Created from basic local rules, the complex behavior can be illustrated using the Vicsek model. Using this model, we have investigated the resulting behavior in terms of different parameters. This exploration provided the foundation of insight into crowd dynamics and jammed conditions. Through research into crowd dynamics, we discovered that the smart particle experienced less force on the indirect path through the crowd making it the better path. By testing various rules of particle interaction, we discovered a rule that produces ordered movement based on topological interaction in a jammed condition with partially periodic boundaries.

1 Collective Motion



(i) The flight of a murmuration of starlings. (See image reference [3])



(ii) A swarm of bees on a branch. (See image reference [2])



(iii) A school of fish spiraling. (See image reference [5])

Collective motion is a phenomenon that has been observed for thousands of years, but has only recently been studied in depth. It is ordered movement within a system that contains many agents that are following local rules. These local rules produce different global behaviors. These rules, while typically simple, produce complex behaviors.

One example of organisms that display complex behaviors from simple rules is locusts. Locusts travel across an area of land and will eat all of the food that they find leaving the land barren. However, once they finish the food within that area, they need more nutrients to keep them alive. To get these nutrients the locusts will start to nip at each other in an attempt to eat their forward neighbor. The affected forward neighbor will begin to move forward more quickly in an effort to get away from being eaten, but also to attempt to eat the locust in front of them. This results in a strong and continuous forward motion from all of the locusts producing a swarm. The complex

behavior of the locusts marching forward is produced from the simple rules of cannibalism and surviving. When this is generalized, it can be seen that simple rules creating collective motion can be modeled using basic mathematical tools.

2 Vicsek Model

As a starting point for our exploration of collective motion and agent-based modeling, we first turned to the Vicsek model, the base model for the motion of self-propelled particles.

$$\theta_i(t + \Delta t) = \arg \left(\frac{\sum_{j \in R_i} \mathbf{v}_j}{\left| \sum_{j \in R_i} \mathbf{v}_j \right|} \right) + \eta \zeta(t) \quad (1)$$

$$\mathbf{v}_i(t) = \langle \cos(\theta_i(t)), \sin(\theta_i(t)) \rangle \quad (2)$$

The Vicsek model describes the motion of N self-propelled particles with time-discrete dynamics dictated by two terms: alignment and noise. The first term dictates alignment. In this term, each particle's orientation is set as the direction of the sum of the direction vectors of particles within a set radius of itself. Then a noise term is added, which is a random angle from a uniform distribution of angles within a set range. Depending on the coefficient η chosen (between 0 and 1), this distribution of angles can have a width as narrow as 0 or as wide as between $-\pi$ and π .

$$\mathbf{x}_i(t + \Delta t) = \mathbf{x}_i(t) + \mathbf{v}_i(t) \Delta t \quad (3)$$

All of the agents' directions are simultaneously updated (using equation (2)) and then their positions are simultaneously updated (using equation (3)). The magnitude of all of the velocity vectors remain constant at 1. In our numerical simulations, we employ periodic boundary conditions to minimize finite size effects. For the sake of simplicity, we kept the values of Δt and the radius of detection at 1.

2.1 Order

Order is a property inherent in the Vicsek model, which describes how similar the directions of the agents are. To measure this quantity in a Vicsek system we calculated, at each iteration, the general alignment throughout the system using equation (4). This is given as the average normalized velocity of all the agents in the simulation. Since in the basic Vicsek model, all particles move with unit velocity, this magnitude must necessarily be between 0 and 1, with 0 occurring ideally when particle orientations are uniformly distributed about the unit circle and 1 occurring when all particles are moving in the same direction.

$$\phi(t) = \left| \frac{\sum_{i \in N} \hat{\mathbf{v}}_i(t)}{N} \right| \quad (4)$$

The order parameter, graphed against time, can be divided into 3 phases: nucleation, coarsening, and homogenization. These behaviors occur in sequence, as seen in 2i and 2ii.

Nucleation occurs as particles rapidly form into small clusters, aligning with their immediate neighbors in small, disconnected clusters (see 2iii). As these clusters move and collide with other clusters, they tend to gain a common direction. This process, called coarsening, corresponds with an increase in global order as the number of distinct directions in which particles move decreases. At the end of the coarsening phase, particles are all moving across the screen, with one or more bands of relatively high particle density moving like waves across the field (see 2iv). Finally, in the homogenization phase, particles begin to spread out across the simulation space due to the influence of the random noise (see 2v). Generally the order parameter converges and remains consistent throughout the homogenization phase. Note that the nucleation phase is much shorter than the coarsening phase, which is in turn shorter than the homogeneous phase.

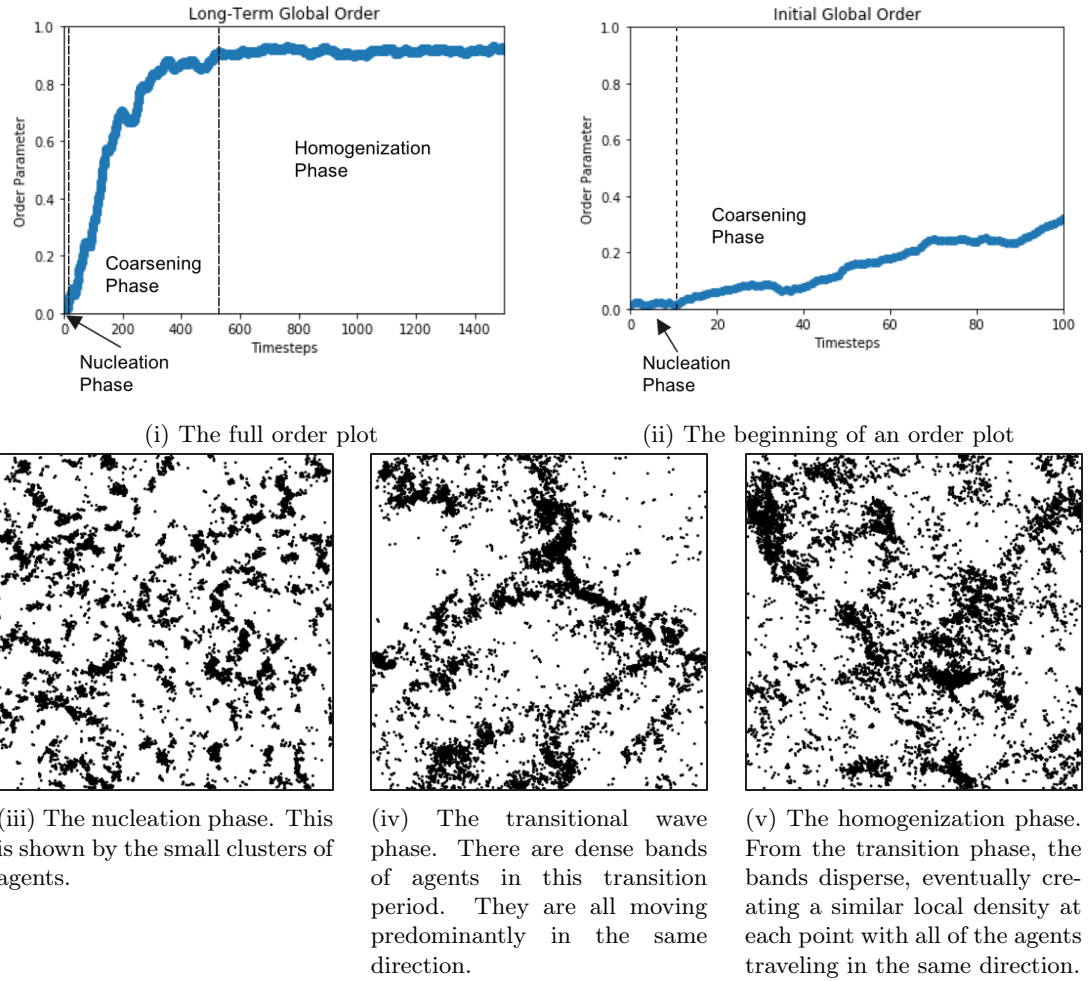


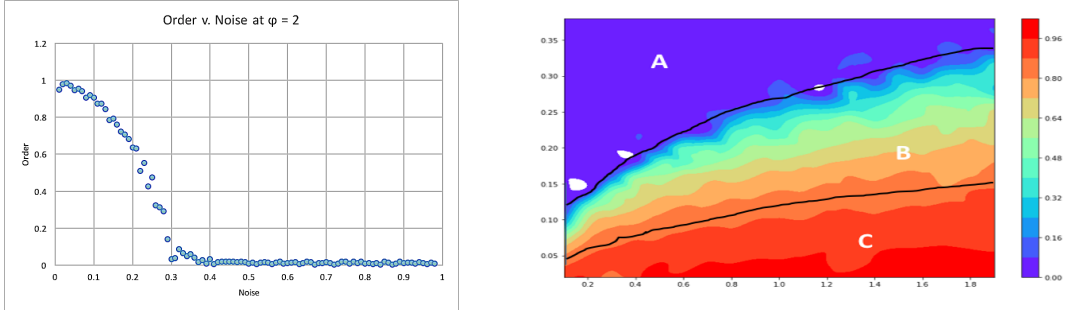
Figure 2

2.2 Parameters

The noise parameter is the random deviation from the angle of alignment for each agent, with strength controlled by the coefficient η . It has a marked effect on the order of the particles: when a simulation has reached its final, homogenized state, its order parameter will hover around a constant which is negatively correlated to the magnitude of the noise coefficient. However, this correlation is not a perfect inverse relation. For a set density value, the final order state varies with η , the noise coefficient, as seen in 3i. Note the sudden drop off in order. This occurs at the phase transition, which is the point at which the noise parameter is able to overcome the ordering effects of the Vicsek rule. In fact, if simulations were run to $t = \infty$, one would expect an almost vertical drop in order at this point. As such, the spontaneous breaking of symmetry and the transition to global order in the Vicsek model should constitute a first order phase transition, meaning that the first derivative of order with respect to noise is discontinuous (due to the expected sharp cutoff).

The effective packing fraction or density is another important parameter of the model. This density is defined as the area of the summed circles of influence about the agents in the simulation, divided by the total area of the system. It is mathematically defined as $\rho = \frac{N\pi R^2}{L^2}$.

The density of the particles is positively correlated with the final order of the system, since as density increases, interactions between particles will necessarily increase. As long as the number of particles within the simulation is sufficiently large, the behavior of two simulations with the same noise coefficient and density will be the same, regardless of the actual number of particles. For this reason, in our experimental design we used a uniform population size of 10,000 and varied the size of the simulated area. It is only at low particle numbers or board sizes that long term behaviors



(i) Relationship between noise and order for a set density value. Notice how order drops down as noise increases.

(ii) Long term order resulting from values of density (x-axis) and noise (y-axis)

Figure 3

of the system deviate from expected values due to finite size effects – errors due to variability that occur with smaller population size.

A unified relationship between noise coefficient, density, and the order parameter can be observed using a heat map (Figure 3ii) which is based on hundreds of simulations run at a range of η and ϕ values.

The heat map is divided into three regions, which represent three distinct phases. Region A denotes the disordered phase, characterized by low densities and high noise values. Here, the long term behavior is a homogeneous distribution of the agents with a lack of global order. Region C denotes the homogeneous phase, which occurs at high densities and low noise values. Here, particles are also evenly distributed, but with high global order. Region B, which separates the two, represents an effective transition region. This band has two characteristic features. First, one observes ordered bands of agents traveling in a disordered background. These bands extend perpendicular to the direction of motion. One expects that these bands give way to an even particle distribution on very large time scales. Second, within this transition region, the characteristic time to reach a final state solution is greatly increased. This is due to the comparable influence exerted by the alignment and noise terms at this transition boundary. As a result, clusters break apart as soon as they are formed, prolonging the onset of collective motion.

2.3 Density Fluctuations

When analyzing the homogeneous, ordered phase, it is worthwhile to consider the extent to which there are density fluctuations of agents. This can provide an intuition for how evenly distributed agents are, and what kind of fluctuations are inherent in their motion. We define density fluctuations ΔN as the standard deviation in number of agents for a given average agent number. This number, N , is given by sampling the number of particles in different boxes for a given box size and averaging over the different samples. For a disordered system, the laws of large numbers tell us that $\Delta N \sim N^{1/2}$. This expectation also has parallels in the theory of random walks, where it is expected that the distance traveled in a random walk scales with the square root of the number of steps. As such, one would expect that as one increases the box size under consideration, thus increasing the average agent number, the fluctuations from this average would scale to the half power. This would be in keeping with our intuition for what constitutes an inherently random process.

$$\Delta N = \sqrt{N^{(2)} - N(d)^2} \quad (5)$$

We measured density fluctuations in our model within both the homogeneous ordered and disordered phases. To do so, we looked at snapshots of boxes centered around the center with sizes $d = 1, \dots, L$ throughout time, where L is the board size. Snapshots were taken on timescales on the order of the board size, to give agents time to move through the system. Average agent

numbers $N(d)$ were calculated by averaging the number of agents in each box of size d throughout time. Similarly, the square averages $N^{(2)}(d)$ were calculated by averaging the number of agents squared in a box of size d throughout time. Corresponding values for ΔN were calculated by the standard deviation (5). As figure 4 demonstrates, when measured for a system in the disordered phase, density fluctuations scaled as $\Delta N \sim N^\alpha$ where $\alpha = 0.5$, as would be expected. Notably, however, when considering a system in the ordered homogeneous phase, we found that $\alpha = 0.8$. This reveals a particularly interesting feature of the Vicsek model class, which is that it experiences giant number fluctuations in the ordered, homogeneous phase.

3 Beyond the Vicsek Model

As we continued researching the Vicsek model through literature, we also read about its myriad applications. Through this we discovered that our primary interests were in crowds and their dynamics. With the assistance of our mentors, we were able to shape our interests into a project with two distinct components – smart agents and jamming behavior. The smart agent component focuses primarily on the implementation of an agent that has more information than the rest, and what the agent can accomplish with that information. The unjamming component focuses primarily on creating topological rules to spontaneously unjam a system while minimizing stress. Both components will require significant changes to the base Vicsek model.

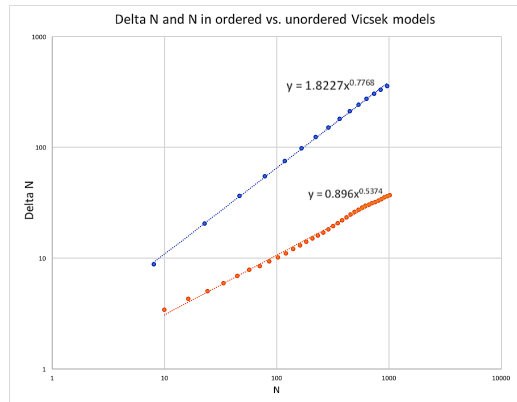
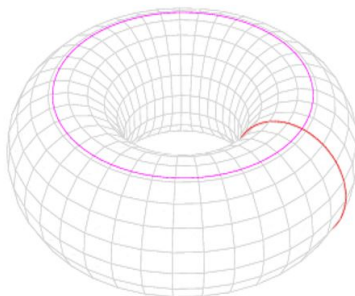
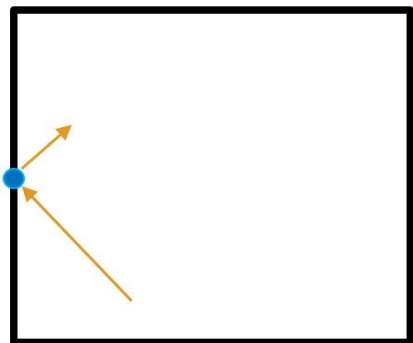


Figure 4: The blue data details the density fluctuations of ordered state while the orange data is the disordered state.



(i) A representation of the continuous boundary as the surface of a 3-dimensional figure. The Vicsek simulation happens on this surface. (See reference [1])



(ii) The arrows show a particle coming into a wall at a certain angle and velocity and being bounced off the wall with the same angle and lower velocity.

Figure 5

One aspect that we will have to change in both is the boundary conditions. The current model has a periodic boundary meaning there are no reflective edges and every edge wraps around represented by figure 5i. If you were to fold a piece of paper, the two long edges would touch at the pink line.

Then the two shorter edges would meet where the red line is.

In the new models, we will need a closed boundary. This new boundary will reflect the incoming direction and will reduce the outgoing speed because the collisions boundaries are not perfectly elastic. The matching angles and reduced speed are represented by the arrows in figure 5ii.

3.1 Crowd Dynamics

Crowds are a natural phenomena that occur frequently when there is one location where a group of organisms desires to be. However, for this classic crowd shape to form there also needs to be a boundary along that location. This could be a herd of cattle trying to exit a pen or a group of humans at a concert. A good example of this would be an event crowd as seen in figure 6i. We want to investigate this type of system by introducing a controlled agent into the system. Our objective is to develop an optimized strategy for infiltrating a crowd with this controlled agent by looking at and understanding crowd dynamics.

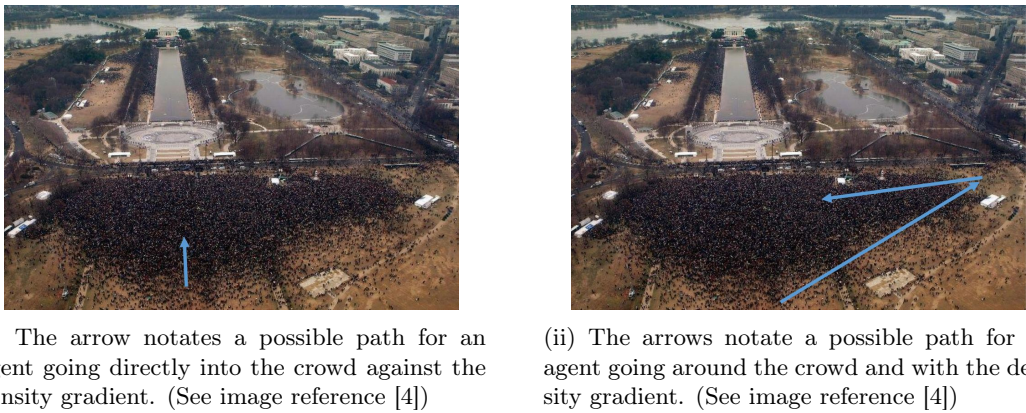


Figure 6

Our crowd is made up of two different classes of agents: naïve agents and smart agents. Naïve agents make up most of the crowd and only have the basic system information of the location of the stage and the positions of the other surrounding agents. The smart agents are the ones that we control. It understand all of the basic information along with an additional piece of information which is our invisible target locations. For our system we introduce a single smart agent to investigate the forces it experiences along its path. The goal of our smart agent is to get as close to our target location as possible using different trajectories. One possible path is a direct path to the front as seen in figure 6i. However, the smart agent could take another path like the one in figure 6ii. If it were to take this path, it would go along the outside of the crowd and enter at the corner going backwards through the crowd. We believe that the indirect path will be easier for the smart agent to accomplish because moving away from the stage allows others to become closer to the stage which makes the crowd more likely to not hinder the smart agent in continuing on its path.

To create a simulation that could assist in modeling such behavior, we must change the underlying dynamics of our system. The original Vicsek model only allows for continual collective motion, but we want a milling crowd which remains relatively stationary but still has some random noise. Initially we chose to use the Langevin's equation of motion ($\dot{\mathbf{p}}_i = -\eta \mathbf{p}_i + \mathbf{f}_i + \langle \zeta_{ix}, \zeta_{iy} \rangle$) to update positions, however due to extreme behaviors we chose to change our base equations to the steepest descent which eliminates the spring like motion seen with Langevin's equations.

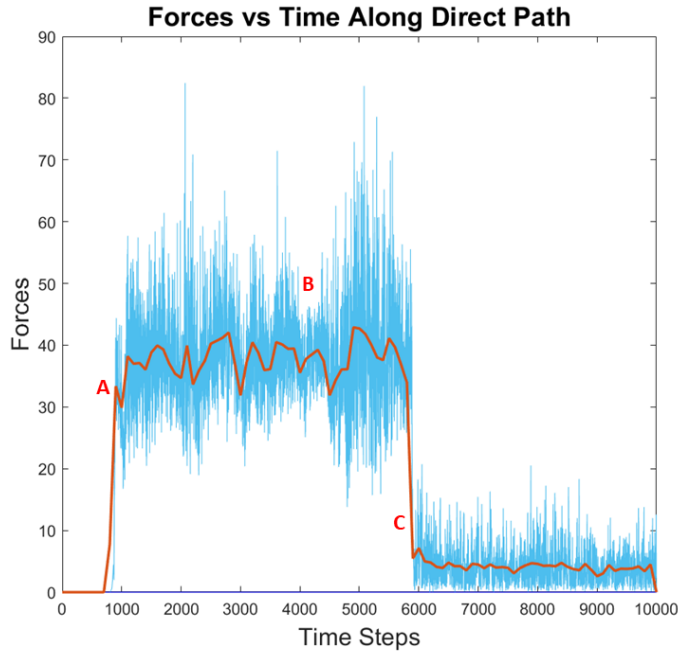
The steepest descent equation (6) is used to move an agent toward the area of least force which for us is the stage

$$\mathbf{x}_i(t + \Delta t) = \mathbf{x}_i(t) - \mathbf{F}_i \Delta t + T \zeta_i \quad (6)$$

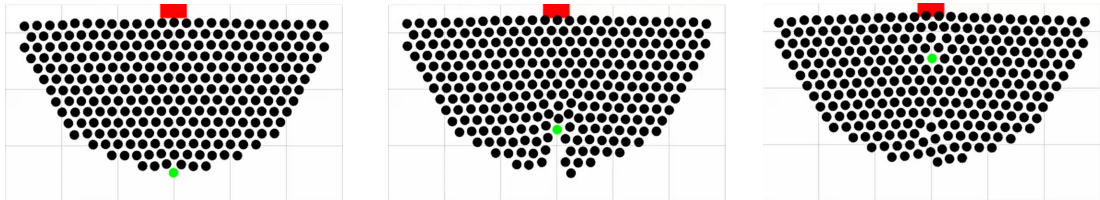
In this equation, we update position based on the previous position($\mathbf{x}_i(t)$), the forces acting on the particle ($\mathbf{F}_i\Delta t$), and a noise term ($T\zeta_i$) which is scaled by temperature. The forces include the Lennard-Jones force (7) and a force towards the stage which the naïve agents experience. The smart agent experiences the Lennard-Jones force (7), but instead of the pull towards the stage, it feels a force towards the target locations. Our random term samples from a Gaussian Distribution, with mean of 0 and standard deviation of 1.

$$F(\|\mathbf{r}\|) = \frac{12\epsilon}{a} \left[\left(\frac{a}{\|\mathbf{r}\|} \right)^{13} - \left(\frac{a}{\|\mathbf{r}\|} \right)^7 \right] \hat{r} \quad (7)$$

We use the classic Lennard-Jones force (7) to model the repulsion over short distances. This repulsion is used for agent-to-agent interaction as well as agent-to-wall interactions. The positive portion prevents overlaps between the agents as well as preventing the agent to exit the system. The negative portion attracts particles toward each other creating the crowd for the smart agent to traverse through. The negative portion is not considered for agent-to-wall interaction since we are assuming that the naïve and smart agents do not want to be stuck near the wall.



(i) Force vs Time graph for the direct path, representing how much force the smart agent experiences throughout the simulation.



(ii) Point A - Smart agent enters crowd.

(iii) Point B - Smart agent in crowd.

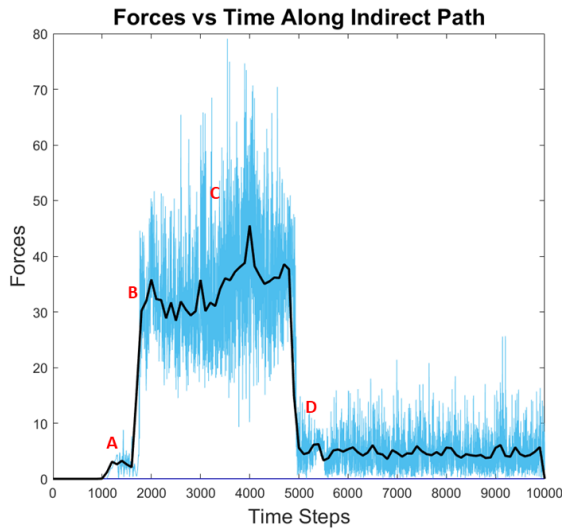
(iv) Point C - Smart agent reaches its goal.

Figure 7

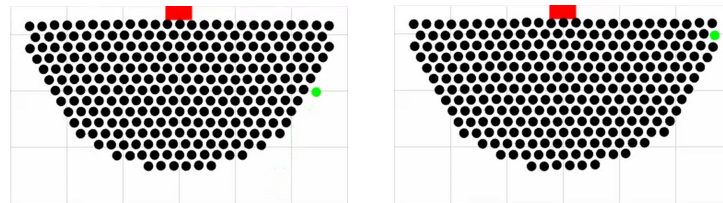
For our simulations, we chose to fix certain parameters. We fixed system size, temperature, and

desired end location of the smart agent. Our system size included 270 particles with 269 of them being naïve agents and one being the smart agent and temperature was set to 15.

The first path we chose to test was the direct path which heads a straight line toward the stage with no angle variation. Figure 7i shows the Force vs Time graph of the force applied on the smart agent during the simulation. At point A (figure 7ii) the smart agent is just beginning to enter the crowd, so the force applied to the agent shoots upwards due to the other agents pushing back on it. At point B (figure 7iii) the agent still is experiencing the higher force due to the fact that the smart agent is continuing to push its way through the crowd toward its end goal. The final point, point C (figure 7iv), has the force drop down almost to zero. It does this because the smart agent has reached its end goal and is experiencing force equilibrium. The small fluctuation appears because of the random noise causing the naïve agents to bump into smart agent.

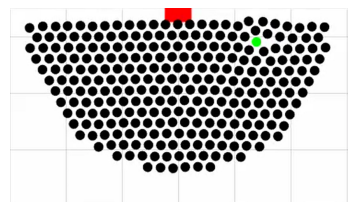


(i) Force vs Time graph for the indirect path, representing how much force the smart agent experiences throughout the simulation.

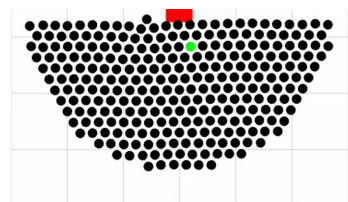


(ii) Point A - Smart agent travels around the crowd.

(iii) Point B - Smart agent enters the crowd.



(iv) Point C - Smart agent in crowd.



(v) Point D - Smart agent reaches its goal.

Figure 8

The next path that we tested with the smart agent was an indirect path, where it skirted the crowd and then entered through the corner to travel backwards towards the center of the crowd. The forces it experienced are shown in figure 8i. With this path, point A is the smart agent traveling around the outside of the crowd 8ii and experiences a small amount of force due to weak repul-

sion interactions between the smart agent and the particles on the outside of the crowd. Point *B* is where the smart agent enters the crowd *8iii*, again causing the forces to shoot up. Point *C* is it pushing through the crowd towards its end goal *8iv*. Point *D* is the final point where the smart agent reaches its end goal *8v*. The forces fluctuations occur again because of the random noise/forces being applied to the smart agent.

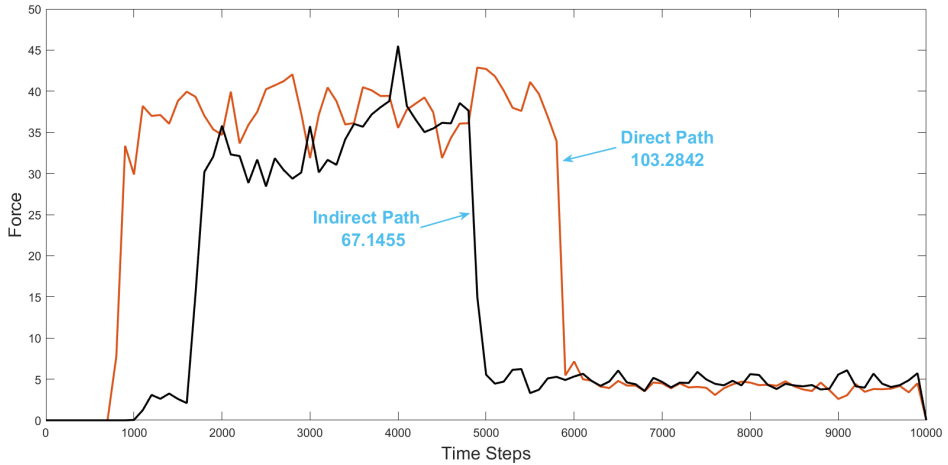


Figure 9: Comparing the Force vs Time curves for the direct and indirect paths. The direct path is represented by the red curve and the indirect path is represented by the black curve. Notice the indirect path showing the smart agent experiencing high forces for a shorter amount of time compared to the direct path.

In figure 9 we are comparing the Force vs Time graphs for both the indirect and the direct paths. It can be seen that the direct path is under a greater amount of force for much longer because it shoots up at approximately time step 1000 and falls back down at approximately time step 6000 where the indirect path shoots up at about time step 1700, and falls back down at about time step 5000. The total force experienced by the smart agent can also be seen from the blue numbers below both the indirect and direct path. It states that for the indirect path the total force experienced is 67.1455, and that for the direct path it is 103.2842. These quantities also clearly express that the smart agent was under a much greater amount of force during its travels in the direct path than it was while traveling in the indirect path.

The pressure gradient diagram, figure 10, represents the difference in pressure at all areas of the crowd. The areas that are more yellow represent the areas of higher pressure. The more mellow, blue colors represent areas of lower pressure. This assisted in showing why the smart agent had an easier time entering through the top corners and traversing backwards instead of pushing up through the middle. The diagram allows us to begin to understand the pressure gradient existing in our system. This displays what we believe to be the reason that the different paths have different amount of force applied to the smart agent.

We believe that there is still much to explore within this model for crowds. We plan to investigate different levels of noise, scaling up the system size and introducing multiple smart agents in one simulation. Our initial investigations indicate that the best path for the smart agent (defined by the path of least force on the smart agent) will change as the noise in the system increases. We

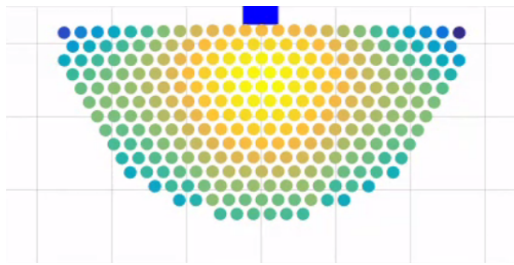


Figure 10: Pressure Gradient Diagram: Depicts the pressure at each point throughout the system. Blues represent lower pressures to yellows that represent higher pressures.

would like to investigate this further to understand the relationship between forces on the smart particle, noise, and path length.

3.2 Unjamming

Our other objective is to develop topological and local rules to spontaneously unjam a jammed system while minimizing stress. We define a jammed condition intuitively, as a state in which particles are unable to move outside of a small radius about their initial position. Stress represents the notion of physical strain and collisions between agents. As such, we seek to investigate what factors can be changed to minimize stress and facilitate quick transition to uniform motion.

To begin, we needed to produce a jammed system. This would be impossible within the constraints of the classic Vicsek model. The two competing terms - alignment and noise - only allow for two long-term states: order in an alignment-dominated regime and disordered movement otherwise. As a result, we turn to a modified Vicsek model, which consists of the removal of the noise term, and replacement with a repulsion term (see equation (8)).

$$\mathbf{v}_i(t + \Delta t) = v_a \frac{\sum_{j \in R_{a,i}} \mathbf{v}_j}{|\sum_{j \in R_{a,i}} \mathbf{v}_j|} + v_r \sum_{j \in R_{r,i}} \frac{\mathbf{x}_{ij}(t)}{|\mathbf{x}_{ij}(t)|} \quad (8)$$

$$\nu = \frac{v_r}{v_a} \quad (9)$$

Here, the alignment and repulsion terms are weighted by the respective velocities v_a and v_r . The radii of alignment and repulsion can vary, but, to begin, we have chosen $R_r = 1$ and $R_a = 2.5$. In this modified model, the relevant control parameters are the velocity ratio ν (9) and the packing density $\rho = \frac{N\pi R^2}{L^2}$, where L is the board size. As with the classical Vicsek model, we created a phase diagram, plotting global order as a function of the control parameters ν and ρ . The resulting heat map, pictured in 11i, demonstrates that, unlike the classic Vicsek model, global order varies independent of packing density, with the onset of disorder at $\nu \approx 0.8$. As such, this repulsion-based model demonstrates significantly different dynamics, with agents exhibiting a tendency to align into local crystalline or hexatic order, especially at high values of ν and ρ [25].

In keeping with these results, we found jamming behavior at high packing densities in a repulsion-velocity dominated regime. A snapshot of this behavior can be seen in Figure 12. The most visually "tight" simulations - those that exhibited the least individual diffusive motion - occurred at low values of v_a and v_r , analogous to low system temperatures. In light of this, the jamming condition seems to be similar to atoms in a solid.

To determine the extent to which particles align in a crystalline structure, as opposed to a fluid state or as an amorphous solid, we explored hexatic order as a function of the parameter space. Hexatic order is defined as $\Psi = |\mathcal{N}_i|^{-1} \sum_{j \in \mathcal{N}_i} e^{i\theta_{ij}}$, where summation extends over all topological (Voronoi) nearest neighbors and θ_{ij} is the angle between particles i and j relative to an arbitrarily chosen reference axis [25]. The variation in global hexatic order can be seen in 11ii, where a maximum is achieved for large packing fractions ρ in a repulsion-dominated regime, in agreement with the findings in [25].

In contrast however, we found significant global hexatic order even at low packing densities. Here,

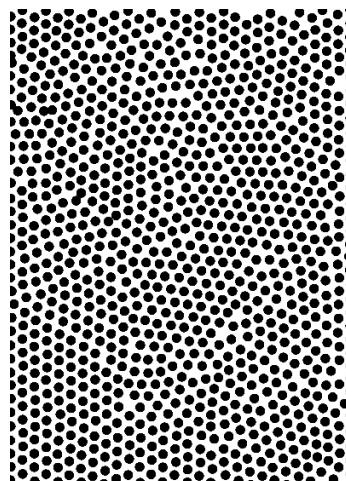


Figure 12: Example of a jammed condition. Several regions in which the particles pack hexagonally can be seen.

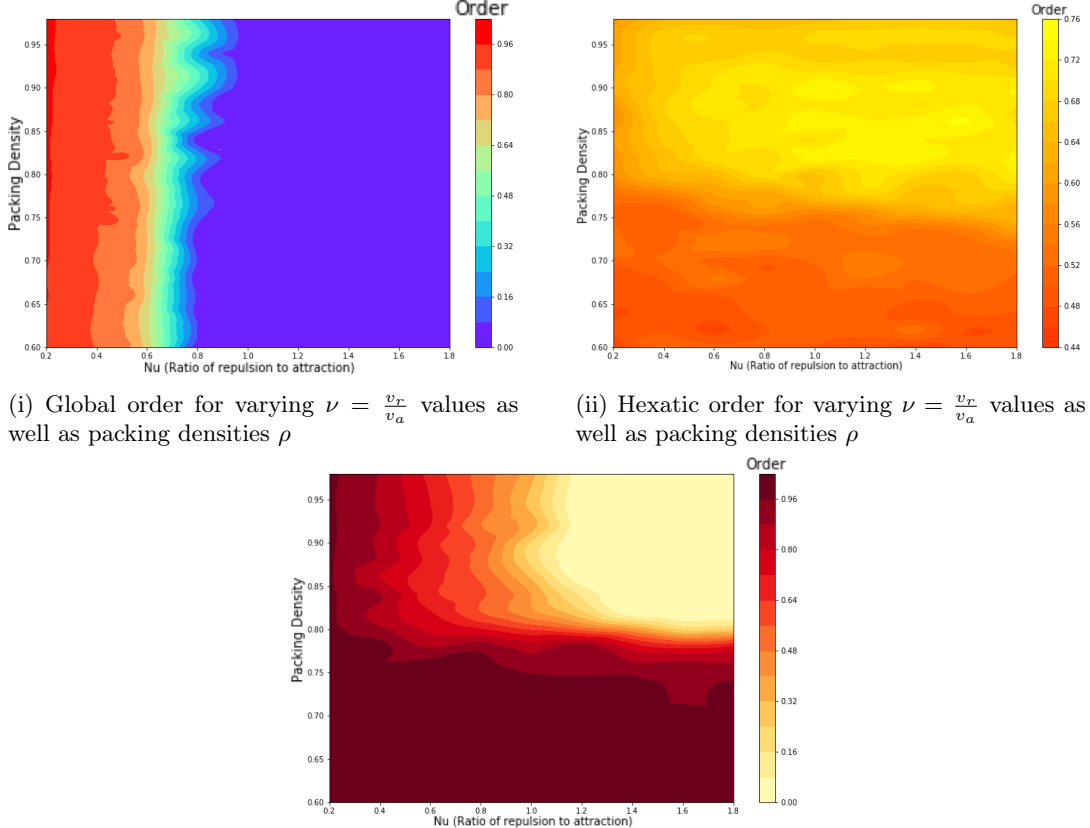


Figure 11: Phase diagrams comparing long term order based on values of ν and ρ

one would usually expect liquid-like behavior with low global hexatic order. This discrepancy might be attributable to the small system size used (1000 particles) or perhaps to having used insufficiently long time scales for computational expediency.

Having implemented Voronoi nearest neighbors for measuring hexatic order, we elected to implement a modification to our repulsion-based Vicsek model in which the summation for alignment is extended not over metric neighbors, but rather topological nearest neighbors. Of these neighbors, those within a metric distance of $2R$ are factored into the repulsion term, where R is the innate particle radius. As with our previous models, we created a phase diagram of the parameter space, to see whether the particle dynamics were significantly altered in a topological Vicsek model. Initially, we expected the dynamics of the topological model to be largely comparable. As is illustrated by 11iii, this intuition was confirmed for packing fractions $\rho > 0.75$. Here, as in the metric model, global order is largely invariate with packing fraction, instead dropping off with increasing values of ν . A departure from the dynamics of the metric model can be observed for $\rho < 0.75$. Here, the system uniformly achieves complete order, regardless of the ratio of alignment to repulsion. Despite differing from the behavior of the metric model, this seems to fit with the nature of our topological model. The alignment term is density-independent, as agents will always have nearest neighbors. At low densities, particles will rarely come within the metric repulsion radius. As a result, we see global order regardless of the value of ν .

While we have defined jamming intuitively as a lack of collective motion and global order, this is an incomplete description, since disordered movement and jammed particles will have an approximately equal global order parameter. Therefore, another parameter used to measure the objective presence (or lack) of a jam is mean squared displacement across all agents. To calculate this, the mean of the squares of all total particle displacements (see equation (10)) is calculated (if a particle goes through a periodic behavior, displacement is calculated as though it had not).

$$MSD(t) = \frac{1}{N} \sum_{i=1}^N ||\mathbf{x}_i - \mathbf{x}_0||^2 \quad (10)$$

In a simulation exhibiting collective motion, the mean squared displacement increases quadratically since each particle's displacement increases more or less linearly. However, in a jammed condition, the mean squared displacement can be seen to increase linearly, with a slope less than 1.

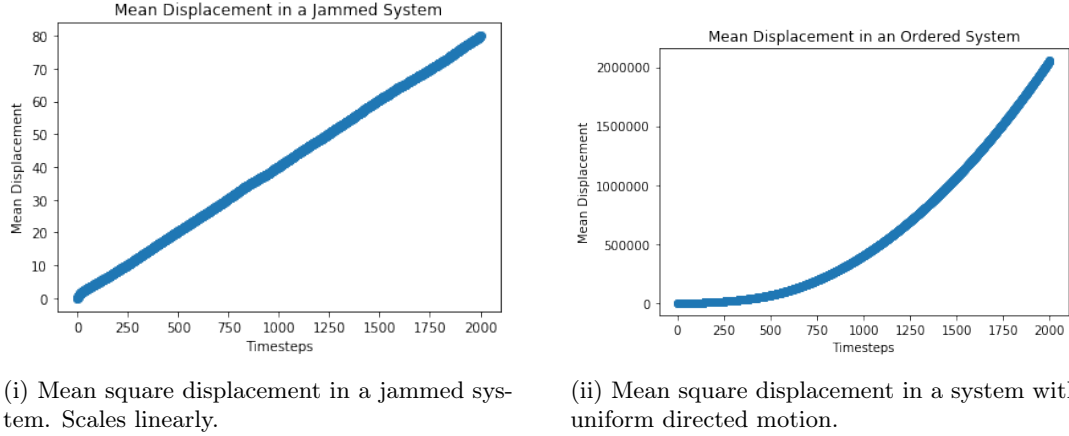


Figure 13: Notice the y -axis scales are different due to different orders of magnitude.

However, we ultimately chose to define a "jam" as a region of the parameter space, rather than as a function of a precise metric. Figure 11iii, displays a schematic diagram splitting the previous phase diagram for the metric repulsion-based Vicsek model into four regions of general behavior. The upper right quadrant corresponds to where the system forms a crystalline solid with high hexatic order. It is this solid state that we are interested in, and in which we hope to induce unjamming through collective behavior.

As we finished these preliminary explorations, we turned our attention to the central problem of finding an optimal unjamming strategy, within the constraints of the repulsion-based Vicsek model. We decided that the best way to approach this problem was to adopt a new rule, by introducing a new parameter, to generate hexatically aligned order in a simulation with values of ν and ϕ that would normally produce a jammed state. In searching for such a rule, we elected to work within a simulation space with particular boundary conditions. The left and right boundaries were reflective, while the upper and lower boundaries had simulated "particle baths" feeding into each side. This choice was made to capture the notion that it should be "new" particles entering the simulation, rather than a fixed number of particles rotating through a periodic boundary. In practice, this was implemented by having particle orientation, \mathbf{p} (15), randomized as particles pass through the periodic boundary.

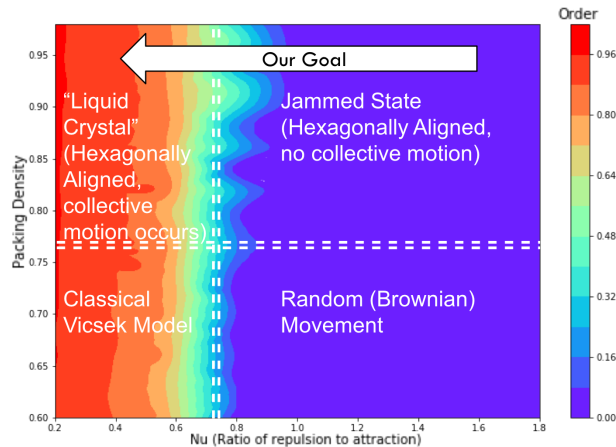


Figure 14: Regions of particle behavior within the repulsion-based Vicsek model. Our goal is to achieve behavior similar to the "Liquid Crystal" region within parameters of ν and ϕ that would normally create a jammed state.

The main rule we decided to implement to create collective motion is based on alignment with the border. Each particle i has an inherent angle, θ_i the direction of which is updated (see equation (11)) based on the particle's direction with respect to the reflective boundaries: if the particle i is moving generally upward, θ_i will be pointing upwards, and if i is moving downward, θ_i will be pointing downwards. θ_i also has inherent noise, which is uniformly distributed within $\pi/3$ radians of the pure upward or downward direction. This term is updated on the Δ' time scale, which is 10 times less frequent than the frequency of position updates, to model an agents' inability to constantly monitor other agents.

$$\theta_i(t + \Delta't) = \frac{\pi}{4} \text{sign}(\mathbf{p}_{y,i})\zeta(t) \quad (11)$$

$$\Delta' = 10\Delta \quad (12)$$

The magnitude of θ_i 's contribution to the movement of agent i is determined by the alignment of the agent's boundary orientation, \mathbf{b}_i , with the average direction of its topological neighbors, using an inner product (see equations (13) and (14)). The more the average direction of the agent's neighbors aligns with its perception of the boundary, the more \mathbf{b}_i will contribute to the agent's orientation. The resulting weight, $w_{b,i}$ is used in (15) to linearly scale the boundary term when calculating the orientation of agent i at each time step. The agent's topological neighbors are given by arbitrarily choosing three other agents from the system. Three was chosen to demonstrate that our rule has a suitably low reliance on topological interactions. Further exploration is required to determine what effect varying the number of topological neighbors has on system dynamics.

$$\mathbf{b}_i(t) = \langle \cos(\theta_i(t)), \sin(\theta_i(t)) \rangle \quad (13)$$

$$w_{b,i} = b_{max} \left| \mathbf{b}_i \bullet \sum_{i \in \tau} \mathbf{p}_i(t) \right| \quad (14)$$

As such, total orientation of the given particle i is then determined using the contribution of the alignment, repulsion, and border-rule terms (see equation (15)). Rather than determining motion separately using both repulsion and alignment, each particle moves the same amount, v_m , each iteration (see equation (16)). Finally, the positional update is the same as in the traditional Vicsek model once the direction is determined (see equation (17)). Figure 15 provides a simplified explanation of the rule.

$$\mathbf{p}_i(t + \Delta t) = w_a \frac{\sum_{j \in R_{a,i}} \mathbf{p}_j}{|\sum_{j \in R_{a,i}} \mathbf{p}_j|} + w_r \sum_{j \in R_{r,i}} \frac{\mathbf{x}_{ij}(t)}{|\mathbf{x}_{ij}(t)|} + w_{b,i} \mathbf{b}_i(t) \quad (15)$$

$$\mathbf{v}_i = v_m \hat{\mathbf{p}}_i \quad (16)$$

$$\mathbf{x}_i(t + \Delta t) = \mathbf{x}_i(t) + \mathbf{v}_i(t)\Delta t \quad (17)$$

$$\psi_R(t) = \left| \frac{\sum_{i \in n} \mathbf{v}_i(t)}{n} \right| \quad (18)$$

See Figure 16 for illustrations of particle positions and directions based on these rules.

To determine the effect of the border rule, we compared metrics including global and local order, as well as stress, for simulations that were identical aside from the implementation of the rule. The border rule was only activated after simulations had run for 500 iterations to ensure a jammed state had been reached.

The changing global order of the simulation, especially when compared to a simulation without the new rule, reflects a significant increase in global order due to its introduction, as seen in figure 17. The two graphs are from simulations with mostly identical parameters: $\nu = 1$, $\rho = 0.87$. The only difference is the introduction of the boundary term, which corresponds with a significant increase in global order.

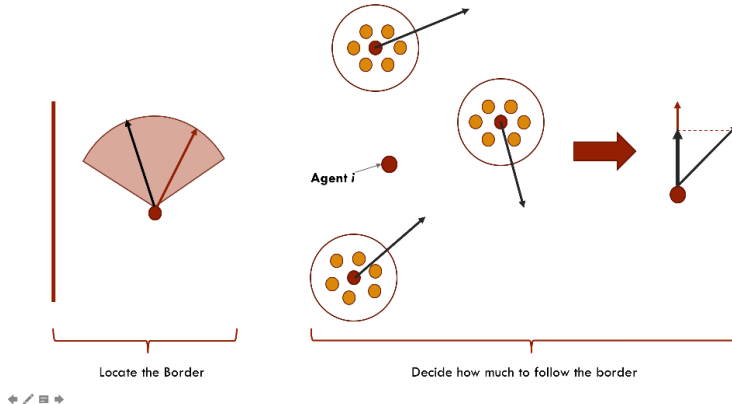


Figure 15

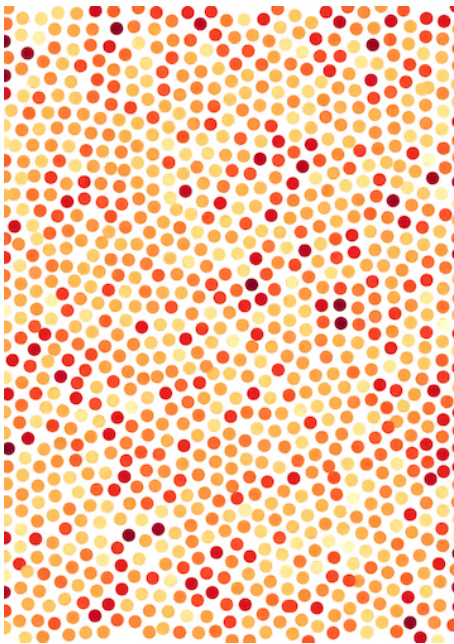
Figure 18 predicts the long-term global order of a system based on ν and the border rule. A clear boundary can be seen between the lower region, where long-term order does not come about, and the upper region in which it does. In the creation of 18, all runs were done at a packing density of $\rho \approx .87$. As a result, all the values of ρ and ν used correspond to the "jammed state" outlined in figure 14. This demonstrates that the boundary rule effectively induces a shift in the phase diagram presented by the repulsion-based Vicsek model, inducing global "liquid crystal" collective motion in an otherwise jammed regime by the introduction of a new term. This term is the maximum border weight, which limits the contribution of the border term in orientation update. In general, for high values of ν , a correspondingly greater border weight is needed in order to overcome the repulsion term and induce collective motion. That order can be achieved for all values of ν with the border weights < 0.5 demonstrates that our rule does not require a disproportionate, unrealistic weighting of the boundary term.

Another aspect of the model that requires attention is the stress, or lack thereof, within the system. We defined stress as the Mean Particle Overlap: For each instance where repulsion occurred, we recorded particle overlap, given by the ratio of the length of overlap to the distance between the centers of two adjacent particles (R_r). See equation (19): $\Delta_{init} = 2R_r$, and Δ' is the distance between particle centers of overlapping particles. The brackets indicate averaging this quantity over all particles in the system.

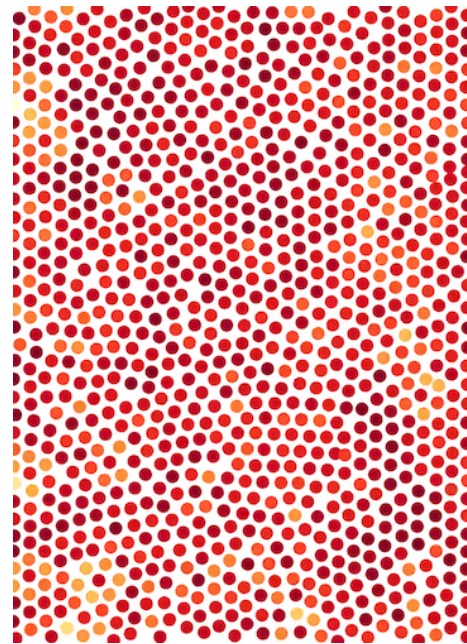
$$MPO(t) = \left\langle \frac{\Delta_{init} - \Delta'}{\Delta_{init}} \right\rangle \quad (19)$$

The introduction of the border rule corresponds to a small increase in stress in the simulation with aforementioned parameters $\nu = 1, \rho = 0.87$. See figure 19. However, a larger increase in stress can be seen in simulations with a higher value of $\nu = 1.3$ and a correspondingly higher border weight of .4 (see figure 20). The relationship between stress and system parameters is illustrated in 21. As would be expected, stress seems to correlate with an increased border weight, as it reduces the strength of the repulsion term, which limits ability of the agents to avoid overlap. As a result, inducing collective motion in repulsion-dominated regimes usually corresponds to higher cumulative stress, since a larger border weight is needed. As we look to expand on our rule and develop new ones, we hope to find a rule that minimizes this stress.

Another property we explored is the local order parameter. Local order, as seen in equation (18) is a measure of the average alignment between a particle and its immediate neighbors. Local order is a useful metric to apply to the new rules we considered for the model, since it demonstrates the presence of collective motion in a regime where collective motion occurs for some, but not all, of the particles in the simulation. In the primary rule we considered, movement parallel with the non-periodic boundaries for a given particle increases with nematic alignment with topological neighbors, but this nematic alignment can be in opposite directions. A possible resultant behavior is the emergence of two or more bands of opposite-aligned particle movement that span the vertical



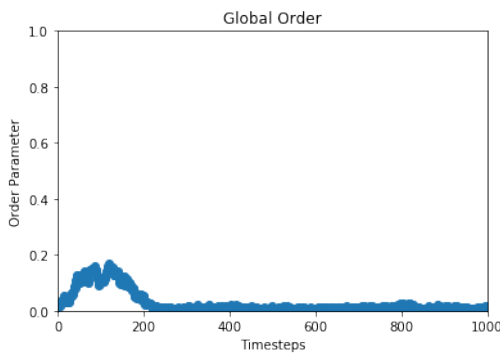
(i) Without Border Rule



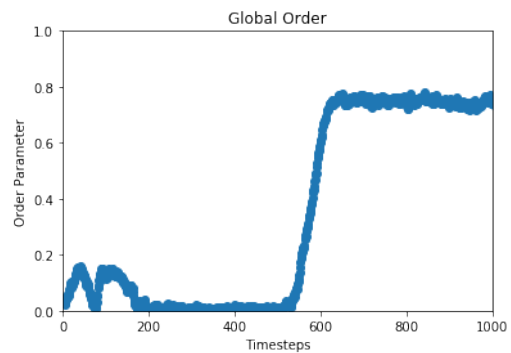
(ii) With Border Rule

Figure 16: Darker colors indicate higher local order, and therefore increased unidirectional movement.

length of the system. The intrinsic alignment of such behavior is not captured by the global order parameter, but is conveyed by the local order. Figure 22 demonstrates a case in which local order increases despite the global order parameter remaining low.



(i) Global order in a jammed system. The small increase in order at the beginning of the simulation is attributable to movement from a random distribution to a homogeneous, jammed state.



(ii) Global order in a system with the addition of the boundary rule. The rule is activated after the particles have reached a jammed state, at timestep 500.

Figure 17

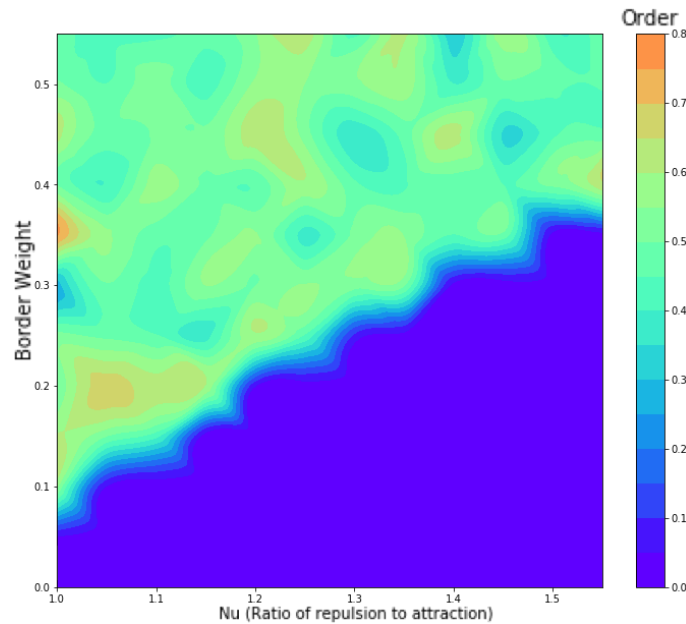
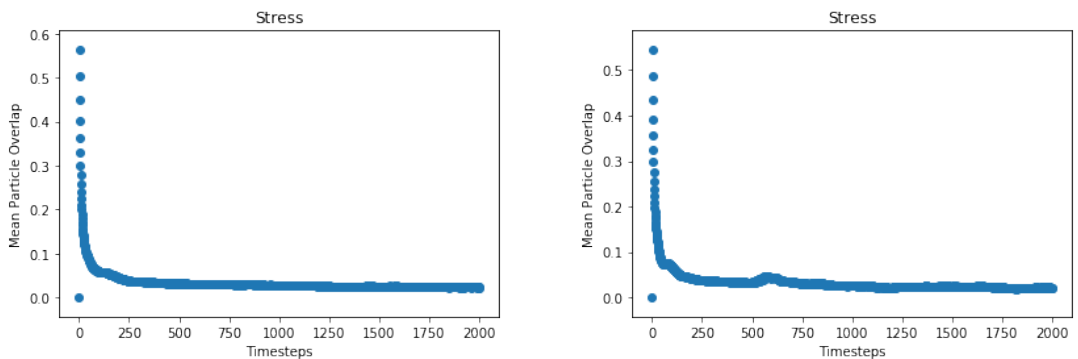


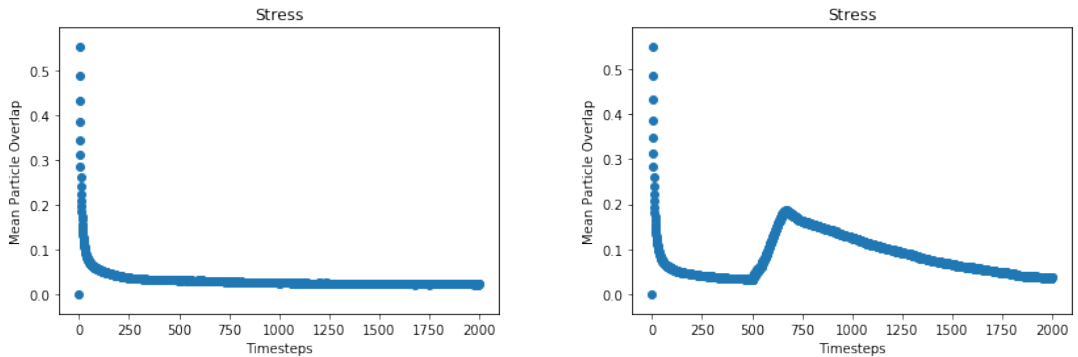
Figure 18: Long-term Global Order as a result of values of ν and the weight of the border term.



(i) Stress in a jammed system. High stress at the beginning of the simulation is attributable to random particle distribution. It quickly gives way to lower values as the particles become homogeneous.

(ii) Stress in a system with the addition of the boundary rule. As before, the rule is activated at timestep 500. Shortly after this timestep a small increase in stress can be seen.

Figure 19: Comparison of stress in systems with $\nu = 1$



(i) Stress in a jammed system with $\nu = 1.3$.

(ii) Stress in a system with $\nu = 1.3$ and the implementation of the boundary rule.

Figure 20: Comparison of stress in systems with $\nu = 1.3$

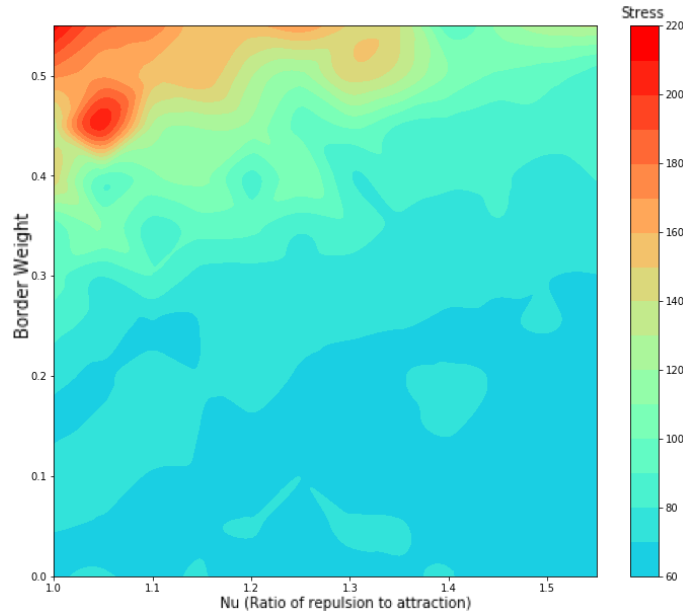
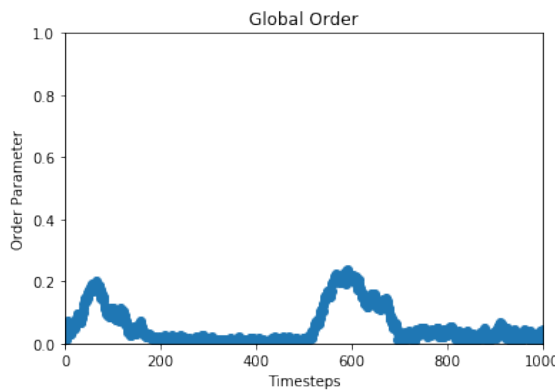
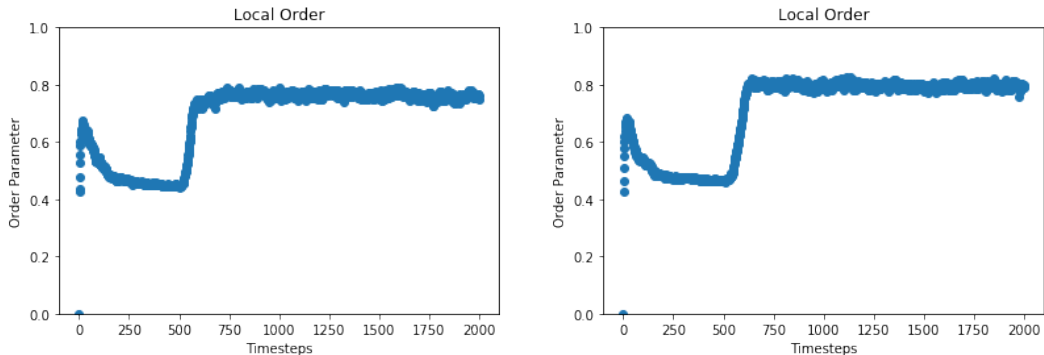


Figure 21: Stress at $t = 1000$ as result of values of ν and the weight of the border term.



(i) Global Order in a boundary rule system which produced multiple bands of opposite-directed particles. Since the bands balance each other out, the global order parameter approaches 0.



(ii) Local order in the bands-behavior simulation.

(iii) Local order in a typical implementation of the boundary rule which produces high global order.

Figure 22

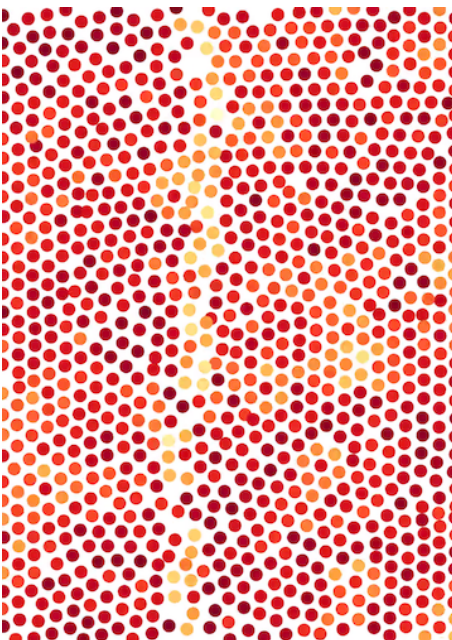


Figure 23: Snapshot of positions and directions for particles in a simulation that exhibited band behavior. Note that particles on the left tend to move down, and those on the right tend to move up. The narrow region of low order indicates the border between these directional regions.

4 Extensions

In the future we will combine these two projects to apply them to real world situations. We plan to investigate a jammed system and how introducing a smart agent will affect the unjamming process. One way we will investigate this situation is with a crowd that has been jammed because of a singular exit point, blocking the flow out. We will observe whether adding a smart agent will help to alleviate the jam or if it will add another body into the jammed mass. A secondary exit scenario we plan to explore is where the room has multiple exits, however all naïve agents are trying to file out of a single exit. With this we will observe if the introduction of a smart agent going out of a different exit will guide a portion of the naïve agents also out of that exit, assisting in unjamming the system.

A second application we will delve into is the jamming and unjamming of cancer cells. To spread, the cancer cells will unjam themselves in the collective motion process known as metastasis. This allows them to break off into small chunks and spread around the body infecting other areas. With this link between cancer cells and collective motion, we believe that smart particles could be introduced to prevent the spread. We would like to investigate the forcing of a system to jam with smart particles.

The tools we developed and used are compiled as a github repository and can be accessed here:
<https://github.com/domleboss97/collective-motion-swarm>

5 Acknowledgements

We would like to thank the Harvard Paulson School of Engineering and Applied Sciences TRi-CAM research program, the NSF grant and Professor L. Mahadevan for sponsoring this project. We would also like to thank our mentors Christoph Weber, Orit Peleg, and Alex Heyde for their valuable knowledge in their field of collective motion and assistance in understanding what interesting questions are. One last person we would like to thank is our advisor Sarah Iams for all of her guidance in mathematical research.

Image References

- [1] Eastaugh, Ben, and Chris Sternal-Johnson. "The Torus." Ferrebeekeeper. N.p., 09 Mar. 2011. Web. 10 July 2017.
- [2] "Honey Bee Facts." Hardy Honey Bee Farms | Sterling Heights, Michigan. Hardy Honey Bee Farms, 15 Oct. 2013. Web. 07 July 2017.
- [3] Lewis, Emily. "A Murmuration of Starlings." Financial Times. N.p., 26 Nov. 2013. Web. 07 July 2017.
- [4] Mei, Gina. "A Visual Comparison of the Crowds at Trump's Inaugural Concert Versus Obama's." Seventeen. N.p., 06 June 2017. Web. 11 July 2017.
- [5] "School Of Fish Pictures, Images and Stock Photos." School Of Fish Pictures, Images and Stock Photos - iStock. iStock, n.d. Web. 07 July 2017.

References

- [1] A. Attanasi, A. Cavagna, L. Del Castello, I. Giardina, S. Melillo, L. Parisi, O. Pohl, B. Rossaro, E. Shen, E. Silvestri, and M. Viale. Collective Behaviour without Collective Order in Wild Swarms of Midges. *PLoS Computational Biology*, 10(7):1–10, 2014.
- [2] C. Bechinger, R. Di Leonardo, H. Löwen, C. Reichhardt, G. Volpe, and G. Volpe. Active particles in complex and crowded environments. *Reviews of Modern Physics*, 2016.

- [3] A. J. Bernoff and C. M. Topaz. Nonlocal Aggregation Models: A Primer of Swarm Equilibria. *55*(4):709–747, 2013.
- [4] P. Blanchard, R. Devaney, and G. Hall. Differential Equations. *Brooks/Cole*, 1998.
- [5] A. Bottinelli, D. T. Sumpter, and J. L. Silverberg. Emergent Structural Mechanisms for High-Density Collective Motion Inspired by Human Crowds. *Physical Review Letters*, 117(22), 2016.
- [6] I. D. Couzin and N. R. Franks. Self-organized lane formation and optimized traffic flow in army ants. *Proceedings of the Royal Society B: Biological Sciences*, 270(1511):139–146, 2003.
- [7] I. D. Couzin, J. Krause, N. R. Franks, and S. A. Levin. Effective leadership and decision-making in animal groups on the move. *Nature*, 433(7025):513–516, 2005.
- [8] J. R. G. Dyer, C. C. Ioannou, L. J. Morrell, D. P. Croft, I. D. Couzin, D. A. Waters, and J. Krause. Consensus decision making in human crowds. *Animal Behaviour*, 75(2):461–470, 2008.
- [9] J. R. G. Dyer, A. Johansson, D. Helbing, I. D. Couzin, and J. Krause. Leadership, consensus decision making and collective behaviour in humans. *Philosophical Transactions of the Royal Society B: Biological Sciences*, 364(1518):781–789, 2009.
- [10] J. Gallian. Contemporary Abstract Algebra.
- [11] F. Ginelli. The Physics of the Vicsek model. *European Physical Journal: Special Topics*, 225(11-12):2099–2117, 2016.
- [12] D. Helbing, I. Farkas, and T. Vicsek. Simulating Dynamical Features of Escape Panic. *794*(July):487–490, 2000.
- [13] D. Helbing, I. Farkas, and T. Vicsek. Simulating Dynamical Features of Escape Panic. *794*(July):487–490, 2000.
- [14] I. Karamouzas, B. Skinner, and S. J. Guy. Supplemental material for : Universal Power Law Governing Pedestrian Interactions. *(C)*:1–7, 2014.
- [15] V. J. Kok, M. K. Lim, and C. S. Chan. Crowd behavior analysis: A review where physics meets biology. *Neurocomputing*, 177:342–362, 2016.
- [16] M. C. Marchetti, J. F. Joanny, S. Ramaswamy, T. B. Liverpool, J. Prost, M. Rao, and R. A. Simha. Hydrodynamics of soft active matter. *Reviews of Modern Physics*, 85(3):1143–1189, 2013.
- [17] E. Méhes and T. Vicsek. Collective motion of cells: from experiments to models. *Integr. Biol.*, 6(9):831–854, 2014.
- [18] N. Shiwakoti and M. Sarvi. Understanding pedestrian crowd panic: A review on model organisms approach. *Journal of Transport Geography*, 26:12–17, 2013.
- [19] J. L. Silverberg, M. Bierbaum, J. P. Sethna, and I. Cohen. Collective motion of humans in mosh and circle pits at heavy metal concerts. *Physical Review Letters*, 110(22):1–5, 2013.
- [20] A. P. Solon, H. Chaté, and J. Tailleur. From phase to microphase separation in flocking models: The essential role of nonequilibrium fluctuations. *Physical Review Letters*, 114(6), 2015.
- [21] V. Tarle, E. Gauquelin, S. R. K. Vedula, J. D’Alessandro, C. T. Lim, B. Ladoux, and N. S. Gov. Modeling collective cell migration in geometric confinement. *Physical Biology*, 14(3):035001, 2017.
- [22] J. R. Taylor. Classical Mechanics.
- [23] K. Tunstrøm, Y. Katz, C. C. Ioannou, C. Huepe, M. J. Lutz, and I. D. Couzin. Collective States, Multistability and Transitional Behavior in Schooling Fish. *PLoS Computational Biology*, 9(2), 2013.

- [24] T. Vicsek and A. Zafeiris. Collective motion. pages 1–85, 2010.
- [25] C. A. Weber, C. Bock, and E. Frey. Defect-mediated phase transitions in active soft matter. *Physical Review Letters*, 112(16), 2014.
- [26] I. Zuriguel, D. R. Parisi, R. C. Hidalgo, C. Lozano, A. Janda, P. A. Gago, J. P. Peralta, L. M. Ferrer, L. A. Pugnaloni, E. Clément, D. Maza, I. Pagonabarraga, and A. Garcimartín. Clogging transition of many-particle systems flowing through bottlenecks. *Scientific Reports*, 4:7324, 2014.